IN-35
177603
P-24

Final Report for Grant NAG8-742

SCIENTIFIC TRADEOFFS IN PINHOLE/OCCULTER FACILITY ACCOMMODATION

Hugh S. Hudson

I. Introduction.

The Pinhole/Occulter Facility (P/OF) consists of state-of-the-art instruments for the study of particle acceleration in the solar corona, and uses a large structure to obtain very high angular resolution. P/OF has been studied in the past as an attached payload for the Space Shuttle, and has been the subject of study by a NASA Science Working Group (P/OFSWG) chaired by H. Hudson of UCSD, E. Tandberg-Hanssen of MSFC (until 1986) and J. Davis of MSFC. Appendix A lists various technical studies and reports carried out under the auspices of P/OFSWG and the Program Development Office of NASA Marshall Space Flight Center.

Under the rationalization of NASA flight opportunities following the Challenger disaster, and the beginning of the Space Station *Freedom* program, the sortie-mode deployment of P/OF seemed less efficient and desirable. Thus, NASA decided to reconsider P/OF for deployment on the Space Station *Freedom*. The technical studies for this deployment continue at the present and will evolve as our knowledge of Space Station architecture and capabilities increase. MSFC contracted with Teledyne Brown Engineering for these technical studies.

II. Work carried out under the grant.

The accommodation analysis generally covered all aspects of the redeployment of P/OF on the Space Station. The particular areas of contribution under this grant included:

- Descriptions of the strawman instrument complement.

- Scientific objectives of the observations.

- Technical requirements of the strawman instruments.

The scientific input to these accommodation studies was particularly important because of the evolving scientific impetus for P/OF. In particular, as a result of the design activity of the GRID instrument for the MAX '91 program, the P/OF scope was enlarged to include γ–ray imaging, *i.e.* to extend the spectral range upwards of 500 keV. This could be accomplished by means of a rotating modulation collimator experiment not included in the original P/OF strawman payload. Such an instrument is described briefly in Appendix B. In addition, a totally new instrument utilizing the P/OF

facility was conceived; this instrument would operate as a Bragg spectroheliograph with one arc-s angular resolution and sufficient spectral resolution to study Doppler shifts and line profiles of solar soft X–ray emission–line sources. Appendix C briefly describes the concept of the Bragg spectroheliograph. We believe that an imaging Compton polarimeter would also be a natural instrument for solar high–energy astrophysics within the P/OF framework, but this instrument was not studied during this period because of lack of time and resources.

The rotating modulation collimator in particular imposes new problems for accommodation on the Space Station. If selected, this instrument would have a considerably larger moment of inertia (up to 10^6 n m^2 for true γ–ray response). This is about one order of magnitude beyond the present requirement for the Payload Pointing Subsystem of Space Station, but its design is not far enough advanced to predict what its performance would be with such a payload under conditions of stable inertial pointing at a celestial target (*e.g. the Sun*), the P/OF operational condition.

III. Conclusion.

This grant supported activities by H. Hudson in the area of scientific objectives and instrumentation for the Pinhole/Occulter Facility as deployed on the Space Station *Freedom*. The results of the full study, being carried out by Teledyne Brown Engineering, are to be found in their reporting. The Space Station appears to be suitable for P/OF deployment in general, and offers extensive capability that would greatly improve P/OF's performance over deployment in the Space Shuttle. These advantages include:

- A massive platform for deployment and pointing of the large ($\sim$50 m long) P/OF boom;

- Ample power and telemetry capability;

- Crew– or robot–assisted deployment, including additional new instruments and refurbishment or change of older instruments or "optics";

- Cryogenic resupply capability;

- On–board calibration of instruments during the observating run;

- Adequate space for the growth of a comprehensive solar observatory around the P/OF instruments.

3

Appendix A. Documents Related to P/OF

I. Technical Reports

'Large–scale Telescopes for X–ray and Gamma–ray Astronomy,' H.S. Hudson and R.P. Lin, 1978, *Space Science Instrumentation* 4, 101.

'The Pinhole/Occulter Facility,' H.S. Hudson, J.L. Kohl, R.P. Lin, R.M. MacQueen, E. Tandberg–Hanssen, and J.R. Dabbs, 1981, NASA TM-82413

'The Pinhole/Occulter Facility: Executive Summary,' J.R. Dabbs, E.A. Tandberg–Hanssen, and H.S. Hudson, 1982, NASA Technical Paper 2089.

'The Pinhole/Occulter Facility,' H.S. Hudson, 1983, *Advances in Space Research* 2, 307.

'Studies with the Pinhole/Occulter Facility,' E. Tandberg–Hanssen, J. Dabbs, H. Hudson, and M. Greene, 1983, AIAA 21st Aerospace Science Meeting, paper AIAA–83–0513.

'The Pinhole/Occulter Facility,' edited by E.A. Tandberg–Hanssen, H.S. Hudson, J.R. Dabbs, and W.A. Baity, 1984, NASA Technical Paper 2168.

'P/OF Phase A Study Report', MSFC/PD, January, 1984 (Appendix E).

'Solar Flares and Coronal Physics,' NASA CP–2421, proceedings of a workshop held at MSFC, May, 1985 (ed. E. Tandberg–Hanssen, R.M. Wilson, and H.S. Hudson).

'Pinhole/Occulter Facility Pre–Mission Definition Study: Payload Concept Trade Studies,' Teledyne Brown Engineering report SP86-MSFC-2952, January 1986.

II. Popular Articles

W.J. Wild, 1987, *Sky and Telescope* (August), p. 126.

G. K. Skinner, 1988, *Scientific American*, (August). p. 66.

Appendix B

A ROTATING MODULATION COLLIMATOR FOR P/OF

B.3.1. Science thrust

A rotating modulation collimator experiment (Schnopper *et al.*, 1968) with cooled germanium detectors would be capable of simultaneous high–resolution imaging and high–resolution spectroscopy for hard X–rays and γ–rays. It would have extraordinarily powerful applications to both solar (see Tsuneta, 1984, for a discussion of the recent successful Hinotori instrument) and non–solar observations. Such an instrument represents the necessary and logical evolution of solar γ–ray and hard X-ray astronomy and would be most appropriate for **P/OF** during the solar maximum of 2002.

With such an instrument, it will be possible for the first time to image flare–accelerated >10 MeV ions, via the prompt γ–ray lines produced by inelastic scatter of those ions in the solar atmosphere. The same instrument will simultaneously image the electrons which produce the hard X–ray bremsstrahlung continuum, allowing fundamental questions such as the following to be addressed:

- Are the electrons and ions accelerated together in the same location or by the same mechanism?

- Is there a separate widespread coronal acceleration of ions, as suggested by the interplanetary energetic particle measurements?

- Is there spatial variation of the spectral distribution of the accelerated ions?

- Is there spatial variation of the elemental abundances in the ambient solar atmosphere?

Similarly, the delayed 2.223 MeV neutron–capture deuterium line and the 0.511 MeV line can be used to image the neutron–thermalization and positron–annihilation regions in flares. The 0.511 MeV line width provides diagnostic information on the temperature, density, and ionization fraction of that region.

In the the hard X-ray (20-200 keV) range the combination of high spectral and spatial resolution will clearly separate the 'superhot' component from the non–thermal power–law impulsive and gradual components.

The sharp breaks in the double power–law flare hard X–ray spectra observed with Ge detector suggest that DC electric fields parallel to the magnetic field may be accelerating the electrons in a manner similar to what happens in the Earth's aurora (Lin and Schwartz, 1987). Mapping of the spatial variation of the break enable us to define the large–scale electric potential structure in the flare.

With the addition of 2–3 layers of bismuth germanate (or other) scintillation detectors behind the Ge, to increase the efficiency at high energies, a modulation–collimator experiment could image energetic 0.1–1 GeV neutrons and 40–130 MeV pion–decay γ–rays, which are produced by the very highest energy ions.

Other potential applications of such exceptionally rich data can be found in the main body of the text.

B.3.2. Experiment description

The rotating modulation collimator system for **P/OF** would consist of a modular array of units as sketched in Figure B.3.1. Each unit would have a simple bigrid tungsten collimator, with a larger one (~50 cm diameter) on the occulter plane in order to provide a full–sun field of view; behind the rear grid would be a set of three or more cooled high–purity germanium detectors in a cryostat, with anticoincidence shielding for background reduction. Each Ge detector would be internally segmented into two segments to allow a wide dynamic range over the hard X–ray γ–ray region from ~10 keV to $\gtrsim$10 MeV (see the detector discussion below). The grids would rotate synchronously, with rotation stability precise enough to keep the grids aligned to a fraction of the fringe width. Counter–rotation of alternate modules would reduce angular–momentum problems.

A set of ten modules would generate ten circular loci in the (u,v) plane, nominally chosen to be at factors of two in slit width starting at 50 microns. This will allow Fourier reconstruction of a high–quality image over a range of angular scales from 0.2 arc sec to about 2 arc min of view. The 30 germanium detectors would have a total area of ~ 1000 cm^2 with effective area of some 250 cm^2, after allowance for the reduced average transmission

due to the grids. Table B.3.1 contains approximate parameters for the **P/OF** rotating modulation collimator experiment.

The grids would be fabricated from tungsten, nominally 4 cm thick except for the 0.2 arc sec (50 micron slits), 0.4 arcsec (100 micron slits), and 0.8 arcsec (200 micron slits) grids where the thickness is limited to 0.5, 1 and 2 cm respectively to maintain full–Sun coverage. Note that the incoming photons need not be absorbed but only scattered a few degrees to miss the entire ten–module detector array. Thus the total interaction cross section from Compton scattering, photoelectric absorption, and pair production — except for a very small fraction of $\lesssim 5°$ forward scatter — is effective, and the imaging can be done up to $\gtrsim 10$ MeV if photon fluxes are sufficient. The depth of modulation for 4 cm thick tungsten grids is 99% at 1 MeV and reaches a minimum of ~95% at ~3 MeV. For imaging of narrow γ-ray lines (Table B.3.2) scattering by more than ~5° will also remove the photon from the line spectral peak entirely. Nuclear collision length in tungsten is 110 g/cm^2, so 4 cm (77 g/cm^2) will provide ~50% modulation for fast neutrons.

Table B.3.2 lists the γ-ray lines, line widths and fluxes expected for a large γ-ray flare. Note that the line to continuum ratio is typically ~1–10 for the prompt inelastic scatter lines. The line widths are typically 5–10 times narrower than the resolution for scintillation detectors. Since the flare continuum below ~ 4 MeV is dominated by electron bremsstrahlung, the high spectral resolution of Ge detectors is required for unambiguous images of the accelerated ions. The total number of counts from a large γ-ray flare (such as April 27, 1981) for a ten–module instrument system is given in Table B.3.2, together with background counts for detectors surrounded by a representative ~5 cm thick bismuth germanate anticoincidence shield and ~25° FWHM field–of–view. For observations of long-lived cosmic sources more massive shielding and background rejection techniques can be utilized to reduce this background significantly.

B.3.3. The germanium detector array

The RMC/Ge detector system (Figure B.3.1 and Table B.3.1) consists of an array of thirty n–type germanium coaxial detectors, each 6.5 cm dia × 7 cm long, the largest n–type Ge crystals presently obtainable in quantity. Three Ge detectors are held in each of ten identical cryostats, each with an attached solid cryogen or mechanical refrigerator. Each cryostat is surrounded by a 5 cm thick bismuth germanate (BGO) annulus and back anticoincidence shield which provides a nominal ~25° FWHM aperture for γ-rays to minimize line and continuum background. The collimation also provides excellent rejection of photons which scatter out of the Ge detectors.

A 3 mm thick passive lead shield in front of the BGO shield absorbs the solar $\lesssim 300$ keV hard X–ray emission so the active shield counting rate is minimized in an intense flare. Fast anticoincidence circuitry $\lesssim 1$ μs overlap time) limits the dead time to $\lesssim 20\%$ even in the largest flares.

Each Ge detector has multiple collecting electrodes which divide it into two distinct volumes, or segments. In the central 1.0 cm diameter hole the top contact collects charge from the front ~1.25–cm segment of the detector, and the long lower contact collects charge from the rear ~5.75–cm coaxial segment. The curved outer surface and top surfaces are implanted with boron to make a very thin (~0.3 micron) window for X–rays, and metallized for the high voltage contact.

The Ge detectors operate in three spectroscopy modes. Photons of low energies ($\lesssim 150$ keV), where photoelectric absorption dominates, are mainly absorbed in the front ~ 1.25-cm segment, while Compton scattered photons and detector background are rejected by anticoincidence with the adjacent rear segment of the detector. Therefore, this mode has the excellent background rejection properties of a phoswich type scintillation counter (Matteson et al., 1977).

Higher energy ($\gtrsim 150$ keV) photons are detected primarily in the thick rear segment alone mode, with a smaller fractions also detected in the front segment and via front–rear coincidences. The bottom segment is shielded by the top segment from low energy, $\lesssim 10^2$ keV photons. This shielding, together with entirely separate electronics for each segment, is crucial for obtaining undistorted high resolution γ–ray line measurements with high efficiency in the presence of intense solar flare hard X–ray fluxes.

In addition, current pulse waveform analysis techniques (Roth et al., 1935; Smith et al., 1988) to eliminate the β^-–decays resulting from cosmic ray activation of the Ge detector are used to reduce the remaining background in the 0.4–2 MeV γ–ray line regions by a factor of 2–4.

The Ge detector front–end electronics are designed to operate over a very wide energy range (20 keV–250 MeV) and to accommodate the wide range of counting rates expected from flare bursts while maintaining the high spectral resolution of the Ge detectors. The BGO shield system, together with the HPGe detectors, can also measure fluxes of high energy (~ 16 to $\gtrsim 250$ MeV) γ–rays and neutrons.

A rotating modulation collimator experiment on board Space Station would have several advantages:

- Access to cryogenic resupply capability or sufficient power (~ 500 watts) for mechanical coolers;

- Sufficient telemetry capability for energy and time–tagging of individual photon events;

- Capability for reconfiguration with different grids, collimators, or even detectors in order to meet different scientific objectives, for example to obtain an ultra–low–background configuration with relatively coarse angular resolution for non–solar observations.

B.3.4 Status of technology

This instrument was not part of the strawman payload for P/OF in past study activities. The period of study requested in this proposal will allow us to bring it to a comparable state of development as other candidate instruments. Specific items needing study and/or laboratory experimentation would include:

- Development of rotating mechanisms and alignment systems.

- Detector development. The two–segment Ge detector has already been developed for balloon–borne experiments. However, adaptation for space flight will require investigation of cooling techniques, etc. A related experiment, consisting of an array of

12 Ge detectors to be used as a high–resolution spectrometer for detection of cosmic γ–ray bursts and solar flare hard X–ray and γ–ray bursts, is being proposed separately as an early attached payload flight investigation for Space Station (K. Hurley, P.I.). We anticipate that the Ge detectors and cooling system from that experiment can be refurbished for use in **P/OF**, while the electronics and scintillator shield can be used without refurbishment. Additional Ge detectors systems will be fabricated to the same design (no new development) to provide the number required for **P/OF**.

- Development of an alternative scanning modulation collimator approach ('dithering') for **P/OF**. In this concept, the grids remain fixed in orientation but one of them executes a circular translation perpendicular to the observing axis. This provides a temporal modulation yielding a single (u,v) point for a given subcollimator, as in the original modulation collimator of Oda (1965).

- Optimization of the geometrical layout of the grids within the constraints of **P/OF**.

Table B.3.1. **Rotating Modulation Collimator**

Number of HP Ge detectors	30
Detector size	6.5 cm diam. × 7 cm long
Number of subcollimators	10
Overall dimension	2 m × 1.5 m area
Energy range	10 keV — 20 MeV; up to 1 GeV with scintillator back shield
Mass	~2000 kg
Telemetry	500 Kbps
Angular resolution	0.2 arc sec
Field of view	whole Sun

Table B.3.2 Solar Flare Gamma-ray Lines							
			Fluences at Earth in FWHM		Counts in P/OF RMC (1000 s)		
Line Energy (MeV)	Excited Nucleus	FWHM (keV)	Lines	Flare Continuum (ph/cm^2)	Line	Flare Continuum	Detector Background
Prompt Lines							
0.429	^{7}Be‡	5	10	9	1.6×10^3	1.4×10^3	80
0.478	^{7}Li‡	10	10	17	1.6×10^3	2.8×10^3	160
~0.45	^{7}Li-^{7}Be‡‡	10^2	20	~170	3.3×10^3	2.7×10^4	1.6×10^3
0.847	^{56}Fe	4.5	5	2	490	190	35
0.931	^{55}Fe	5	2	2	190	190	25
1.238	^{56}Fe	9	2.5	2	190	160	25
1.317	^{55}Fe	13	2.5	2	190	160	25
1.369	^{24}Mg	18	7.5	3	620	230	40
1.634	^{20}Ne	23	13	2.5	880	170	35
1.779	^{28}Si	25	8	2	520	130	35
2.313	^{14}N	54	6	3	360	160	125
4.438	^{12}C	115	10	1.5	410	60	30
6.129	^{16}O	120	10	1	340	30	15
Delayed Lines							
0.511	e^+	2–10	25	—	3.2×10^3	—	
2.223	^{2}H	3(0.1)*	60(4.3)*	—	2.5×10^3	—	3

† The 3σ sensitivity is computed using Poisson statistics for low count cases where appropriate.

‡ Computed for a downward beam or fan beam (see Figure 4).

‡‡ Computed for isotropy (see Figure 4), with flare continuum taken into account.

* This line has an intrinsic width of ~0.1 keV, so the instrument FWHM resolution (3 keV) is substituted. The 2.223 MeV fluence observed for the 27 April 1981 flare is highly attenuated because the flare is located near the limb; the value of 60 is for a comparable flare within ~70° of disk center.

** The background counts include both line and continuum. The sensitivity is computed assuming a narrow (~3 keV) solar 511 keV line.
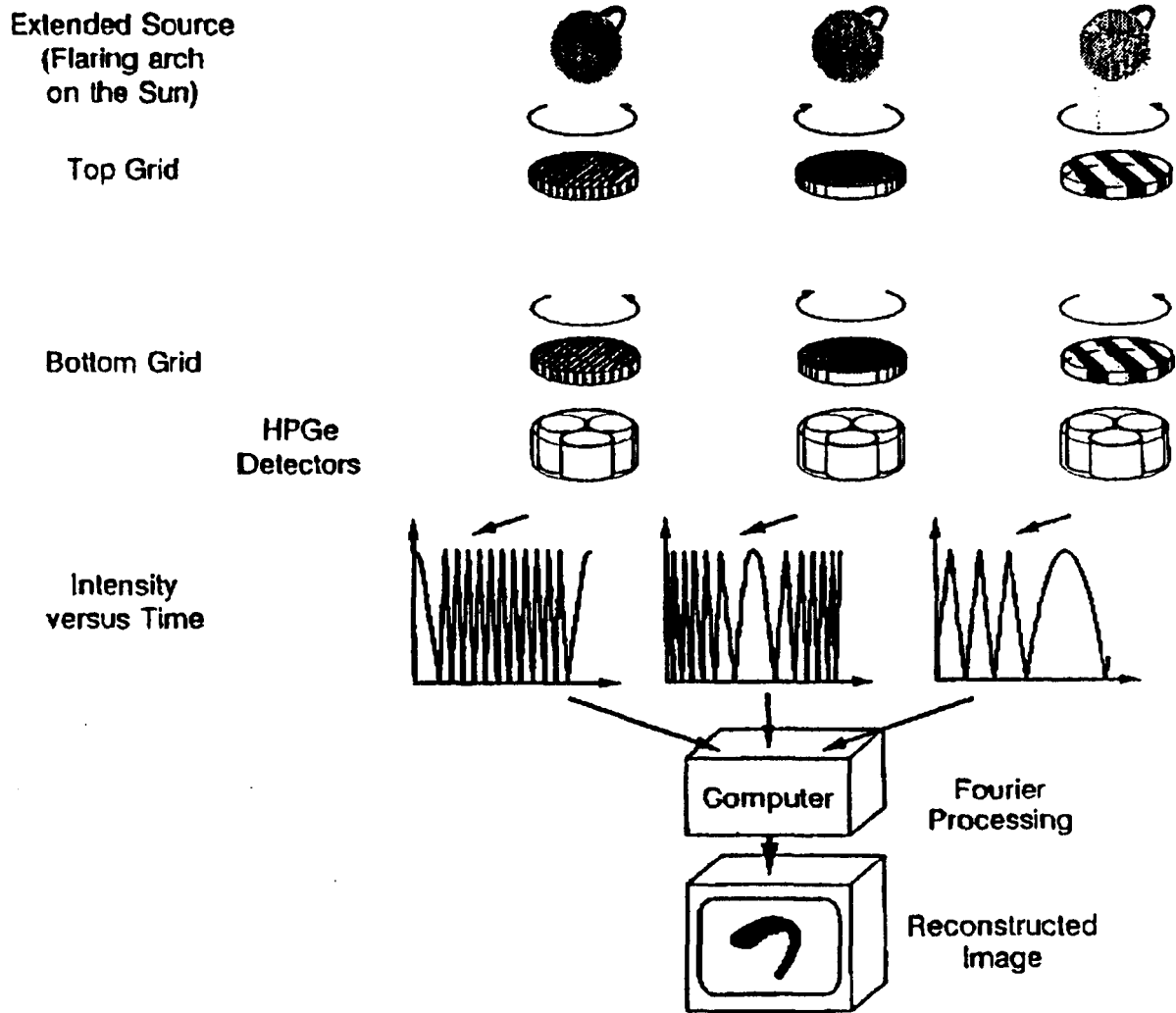
ROTATING MODULATION COLLIMATORS

Figure B.3.1: Schematic view of a rotating modulation collimator instrument for **P/OF**. Each of ten units consists of a pair of synchronously rotating masks, providing temporal modulation patterns as sketched on a set of three high–purity Ge detectors. The modulations give imaging information on circular loci in the Fourier (u,v)–plane, providing excellent image quality.

Appendix C

A BRAGG IMAGER FOR P/OF

B.4.1 Science thrust

The **Pinhole/Occulter Facility** will enable the development of a totally new kind of large–area imaging soft X–ray monochromator with high resolution. This instrument will allow us to study the dynamics of high–temperature plasmas with unprecedented capability. These plasmas include material trapped in closed magnetic loops in active regions, flares, and plasmas in the corona such as coronal transients. The spectral resolution of this device can easily suffice to resolve the detailed structure of the X–ray emission lines, for example of the He–like (FeXXV) and H–like (FeXXVI) ions of iron, giving information on plasma 'turbulence' and Doppler shifts down to velocities of a few tens of km s^{-1}. The angular resolution perpendicular to the dispersion direction will be limited by the diffraction in the coded mask, at 1–2 arc s depending upon wavelength; in the dispersion direction by the rocking curve of the crystal. To eliminate the two–dimensional 'overlappograph' ambiguity of a slitless spectrograph, we need two units with orthogonal dispersion directions.

For non–solar observations, such an instrument offers the possibility of large fields of view with moderate angular resolution (1–2 arc s FWHM) with the diagnostic power of high spectral resolution, providing capability for the study of all of the components of the emission–line complexes; these lines may contain direct information about temperatures and densities. Objects of interest include extended sources such as supernova remnants (including SN1987a?), and discrete sources singly or in clusters.

B.4.2 Experiment description

The Bragg imager consists of a coded aperture at the end of the **P/OF** boom, with a set of crystals in the detector plane, set at proper Bragg angles to scatter photons into large–area position–sensitive proportional counters.

To understand the principle of operation of the Bragg imager, consider the response of a Bragg crystal in wavelength and in angle. The Bragg condition $\lambda=2d\sin\theta$ is, for given λ, satisfied within an annular cone about the direction of normal incidence. The center of this cone is defined by the Bragg condition. The width of the annular ring (in θ) is given by the *rocking curve* of the particular crystal. Except very near normal incidence, the angular diameter of the cone will be much greater than that of the solar disk, or disk plus corona, hence the zone of non–zero response in the solar vicinity will be approximated by a strip with parallel sides. The narrow direction of the strip corresponds to the dispersion direction. Mechanical collimation will determine the extent of this strip, which will almost (but not precisely) follow a great–circle arc. The following explanation of the Bragg imager builds the general case of the performance from some simple cases.

We first consider how the crystal alone responds to a field containing a distribution of multiple point sources with emission lines. Subsequently we consider how the mask modifies that response. To map a large region or to monitor the full solar disk, one rocks the crystal. We ask how the output varies with angle for four specific cases:

1. A single point source;

2. Several point sources geometrically aligned along the dispersion direction, each source emitting at only a single wavelength;

3. Multiple sources, each luminous at a multiplicity of wavelengths; and

4. A distribution of point sources displaced perpendicular to the dispersion direction.

The responses of the crystal and detector (without the coded aperture) will then be:

1. The limiting angles of the rocking excursion define limiting wavelengths λ_1 and $lambda_2$, for a specified point, and the spectrum between these wavelengths is reproduced in the variation of signal with angle as the crystal rotates;

2. The source brightness distribution is mapped out in the response as a function of rotation angle;

3. If there are N point sources displaced in the dispersion direction, each with M lines, these produce N × M signal maxima, whose ordering depends upon the relative spacings in angular position and wavelength (as in an ordinary spectroheliogram);

4. Perpendicular to the direction of dispersion, the crystal performs as a (monochromatic) mirror, hence the source brightness distribution will be reproduced on the detector for photons incident at a single point, but the brightness distribution will be smeared in the dispersion direction according to its spectral distribution.

How is this changed if a mask is placed at a considerable distance in front of the crystal? Suppose the mask contains a coded hole pattern in the perpendicular direction. This will immediately alter case 4 in the above list and permit imaging in that direction. The first three cases will be affected only insofar as the mask restricts the field of view of the crystal, *i.e.* what can be seen at all. Photons from any portion of the field that can still reach the detector will cause the same responses as before.

There are several sources of broadening of these patterns to be considered, and the restrictions they impose will determine what is possible for astronomical imaging spectroscopy. These broadening sources are (i) the natural rocking curve of the crystal; (ii) the thermal or other broadening of the lines studied; (iii) the Doppler shifts of these lines; (iv) diffraction from the mask elements; and (v) misalignment of segments in the case of a mosaic crystal arrangement. Diffraction can be estimated from $\theta \sim (\lambda/D)^{0.5}$, and leads to values of 1–2 arc s for D = 50 m for the soft X–ray emission lines. The Fe complex near 6 keV is the most favorable for study because of the short wavelength, but 2 arc s improves on all previous observations in this wavelength range. The diffraction limit here is the same as for other forms of coded–aperture imaging.

To obtain two–dimensional imaging at the highest diffraction–limited resolution without the 'overlappograph' ambiguity of a slitless spectrograph, we need at least two units with different dispersion directions. Modular construction for different wavelength ranges, different dispersion directions, *etc.*, would make this possible in a straightforward manner.

B.4.3 Status of technology

The Bragg imager is the least–defined of the six instruments considered as candidates for **P/OF**, and the ideas presented here are tentative. Nevertheless, the basic principles of Bragg crystal spectroscopy are well known and have been frequently used in space experiments; the advantages offered by **P/OF** are strictly in terms of the scale of the instrument and the straightforward manner whereby 1–2 arc s spatial resolution can be achieved with the multiplex advantage of two–dimensional detection. The several options for the implementation of the concept need tradeoff analyses with scientific objectives better defined than at present. For example, it would be possible to subdivide the crystal area into regions with different rocking curves or spectral settings, to make the whole instrument rotate to reduce spectral/spatial ambiguity, or to use bent crystals for higher time resolution.

Germanium crystals using the (220) plane near $\theta = 27°$ have been used in previous spectroscopy experiments in space and would work for the Fe lines in this application; the crystals are available in sizes exceeding 100 cm². For a Bragg imager module determined by this crystal size, the spectral range subtended for a flat–crystal application would be on the order of 0.01 Å. For Mg, ADP organic crystals using the (101) plane near $\theta = 52°$ are suitable, and for Si germanium in the (101) plane at $\theta = 51°$.

B.4.4 Scientific program

The scientific program for the use of a Bragg spectroheliograph consists of spectral imaging at a resolving power of $\lambda/\Delta\lambda \sim 10^4$ to 10^5, angular resolution of 1–2 arc s, and great sensitivity because of the large collecting area; the parameters will depend in detail upon the choice of spectral region, crystal, mask configuration, and detectors. The highest resolution will not be available except at the shortest wavelengths, *i.e.* ~ 2 Å. However these properties in general would permit characterization of the physical state and dynamics of solar plasmas to degrees greatly improving on previous observations. High sensitivity implies high time resolution, and one important application of such observations would be to characterize solar plasmas at the moment of 'triggering' of a flare or other eruptive phenomenon. The great sensitivity available from large area may allow **P/OF** to obtain high–resolution spectroscopy of the pre–flare conditions in the plasma, of great importance identifying the physics of the instability.

For non–solar observations, such an instrument offers the possibility of large fields of view with moderate angular resolution, but with spectral resolution capable of producing the maximum amount of diagnostic information about the objects studied. These would include supernova remnants and interstellar shock waves, in which the physical conditions change in interesting ways across the source; and clusters of galaxies, active galactic nuclei, and stars; here the multiplex advantage of the coded–aperture imaging would allow multiple objects to be observed simultaneously.

Appendix B.5

A WHITE-LIGHT/ULTRAVIOLET IMAGER FOR P/OF

B.5.1 Science thrust

The White-Light/Ultraviolet Imager will permit high-resolution polarimetry images of the solar limb and corona in both broad and narrow band wavelengths. The major scientific theme of this instrument is to investigate the physics of coronal substructures. In the past two decades. improvements of the classical observational techniques expanded our knowledge to the point where simple models cannot adequately describe the sun's outer atmosphere: we must now consider inhomogeneous geometrical models such as loops, streamers, and coronal holes. These coronal features are distinguished by their different temperatures, densities, and magnetic field configurations. An unknown nonradiative energy flux interacts with the coronal plasma in each type of feature, and in essence controls its form. While with conventional coronagraphs we could distinguish some characteristics of coronal features at the largest scale, theory and models both demand a much finer spatial and temporal scale to discriminate among competing physical mechanisms which operate in the substructure of various coronal features.

Specifically the White–Light/Ultraviolet Imager on **P/OF** will concentrate upon the following scientific problems:

- Understand the effects of processes that deposit energy and momentum within the substructure of the expanding corona and thereby generate the solar wind.

- Understand the configuration and strength of the magnetic fields in various coronal features.

- Understand the coronal dynamics of processes that deposit energy into the substructure of closed magnetic regions. Specific questions center on who do the properties of coronal loops depend upon their photospheric origins and what is the relationship between prominences and the surrounding corona.

- Understand the plasma processes occurring in adjacent closed and open magnetic–field structures.

- Understand the interactive mechanisms of the plasma and magnetic fields as the corona reacts to slowly–varying conditions on the solar surface.

- Understand the dynamic processes that are responsible foe the expulsion of material from the solar surface in coronal transients and other ejecta. Specific questions concern how non–thermal particles are accelerated in the corona, what propels coronal mass ejections, and are the properties of the coronal plasma controlled by a continuous interaction with a nonradiative energy flux generated by subphotospheric convection or

by a continuum of dynamic "explosive" phenomena such as spicules, macro-spicules, coronal "bullets," microflares, magnetic field reconnection, etc.

The greatest potential for understanding the macroscopic physics of the various open and closed structures in the corona lies in the ability to apply plasma diagnostic techniques at small spatial and temporal scales. This is the central observational thrust of the White-Light/Ultraviolet Imager.

B.5.2 Experiment description

The White-Light/Ultraviolet Imager uses the mask atop the **P/OF** boom as an occulter to block direct emission from the solar disk and to effectively vignette the rapidly-decreasing height dependene of the irradiance emanating from the corona The edge of the **P/OF** mask within the instrument's field of view is serrated to redirect diffracted light away from the telescope optics. Light passing beyond the external occulting mask is intercepted by an all-reflecting coronagraph with a Gregorian primary/secondary configuration. An iris surrounding the primary mirror is adjusted by sensing the position of the edge of the external occulter to assure temporal stability of instrument vignetting and stray light characteristics. The primary mirror forms images of both the corona and the external occulting mask — the latter image being blocked by an internal occulting disk. The coronal image is then reimaged by the secondary mirror, through a polarization analyzer, onto the focal plane. The active secondary mirror provides image stabilization to maintain a 1 arc second resolution during the multiple exposures required for Stokes polarimetry. The scope of this active system depends critically upon the pointing implementation of the **P/OF** system upon the Space Station.

A large back focal distance behind the primary mirror (about 1 m) provides adequate room to mount focal-plane instrumentation. This system permits the use of dielectric filter techniques to isolate individual coronal spectral lines as well as broadband measurements of the electron scattered continuum. Spectral resolution of individual lines depends upon tunable filter systems and the sensitivity of the CCD detection system.

A parallel calibration optical path that has access to direct irradiance to the solar disk is located next to the primary instrument. This subsystem provides an in-flight calibration of the intensity of the coronal light relative to the solar disk. Direct sunlight is allowed to pass through a diffusing opal and a wheel containing different neutral density filters onto the focal plane subsystem.

Electronic control of the instrument is divided into several categories: CCD detector and associated electronics to control the signal chain through conversion to digital values, an instrument computer based controller, storage for digital CCD images, input and output buffer interfaces to the **P/OF** data handling system, and a communication bus among the various components. Digital I/O circuitry controls motors for filter wheels, polarization analyzer, active optics and apertures, and optical path selection as well as monitoring discrete engineering data. A separate microprocessor controls

the CCD waveform generator and transfers digital information from the CCD line memories to RAM memory. The system also includes a real time clock, some count-down timers to monitor instrument functions, and circuitry to control the thermal-electric coolers used to regulate the temperature of the CCD. Because of the large data rates possible from the instrument, intelligent onboard data processing must to applied to the data before shipment to the ground. Thus the operational constraint of data recording or transmission will be the limiting factor for the highest temporal image cadences.

The White–Light/Ultraviolet Imager can be used in three modes: outer coronal, inner coronal, and limb imaging. For outer coronal operations, the telescopic optical axis is pointed to between 1.5 to 2.5 solar radii from sun center while the instrument remains fully within the shadow of the P/OF occulter. To observe inner coronal radiation close to the limb (e.g., prominences, active region coronal loops, coronal rays, etc., the telescopic optical axis is pointed to about 1.1 solar radii and internal occulting apertures are positioned to accept diminished occultation at the expense of a higher instrumental stray light level. The greater coronal signal strengths close to the limb permits higher stray light levels without compromising the signal–to–noise ratio of the measurements. In the third mode, occulter apertures are positioned to permit direct solar disk radiation within 0.05 solar radii of the limb to impinge on the telescope optics while still blocking most of the remaining disk radiation. In this mode, spicules and other dynamic limb phenomena can be studies including and direction and strength of the magnetic field as it expands into the corona.

B.5.3 Development status

The technology for the individual elements of the White–Light/Ultraviolet Imager is well in hand, having the benefit of past space–borne instrumentation. Coronagraphs on OSO's, Skylab, and SMM provide the insight to proper stray light suppression techniques and laser mirror technology provides surface superpolishing required to minimize stray light from reflective surfaces. Mirrors of this size and larger have been produced (an example being the Spacelab Hopkins Ultraviolet Telescope, HUT). Filter technology required has been proven on instruments such as the Spacelab SOUP instrument and CCD are now common place as space–borne detectors. The major issue for the White–Light/Ultraviolet Imager will be its accommodation on P/OF and the aspect sensing of the location of the external occulter atop the boom. From this signal, internal apertures must be adjusted to maintain their relative alignment. The exact implementation of this function requires further study as the complete P/OF system is more fully defined.

Table B.5.1 **White–light/Ultraviolet Imager**

Aperture	50 cm
Angular Resolution	1 arc sec (FWHM)
Image Field of View	16 arc min
Full Field of View	.95 to 3 Solar radii
Spectral Range	1100 to 11000 Å
Temporal Resolution	< 5 seconds
Detector Type	1000 × 1000 pixel CCD
Overall Dimensions	3.5 m × 1 m × 1 m
Mass	200 kg
Telemetry Rate	1 Mbps
Power	200 W

Appendix B.6

AN EUV IMAGER/SPECTROGRAPH FOR P/OF

B.6.1 Science thrust

The EUV Imager/Spectrograph provides a 100–fold increase in telescope collecting area for EUV spectroscopy of the extended solar corona (1–10 solar radii from sun center). The increased sensitivity can be used to improve spectral, spatial and time resolutions or to extend EUV spectroscopy of the extended corona to spectral lines that are too weak to observe with conventionally sized instruments. Such improvements permit, for example, spectroscopic determinations of the chemical compositions, temperatures and outflow velocities of coronal mass ejections and polar plumes. It permits detailed studies of the physical processes responsible for controlling the behavior of a broad range of ions in the accelerating solar wind plasma. The high spectral resolution combined with high sensitivity will provide line profile measurements of a broad range of ions–the mass dependance of the derived velocity distributions, when compared to theoretical predictions, are expected to provide significant constraints on the identification of the physical processes responsible for heating and direct momentum transfer to solar wind ions.

B.6.2 Experiment description

The EUV Imager/Spectrograph is intended to provide spectroscopic diagnostics and image rasters of the solar corona from its base to at least 10 solar radii from sun center. The instrument consists of an externally occulted telescope and a high resolution EUV spectrograph. The external occultation is provided by the **P/OF** mask which shields the telescope from direct illumination by the solar disk. The edge of the mask is serrated to reduce the level of diffracted light on the telescope. The useful size of the telescope mirror is proportional to the separation between it and the mask. Because of the large separation, **P/OF** provides an opportunity to use a much larger telescope mirror than would be possible with a conventionally sized instrument. This permits EUV spectroscopic observations and imaging of the extended solar corona with 100 times the sensitivity, and much higher spatial, spectral and time resolution than is possible with conventionally sized instruments.

An instrument for EUV spectroscopy and imaging of the extended solar corona must overcome several observational difficulties. It must be situated in space because of the absorption of EUV radiation by the atmosphere. It must detect intensity levels that are typically 10^{-6} to 10^{-8} of the levels on the solar disk. The optical system must reduce the stray light backgrounds from solar disk light to levels that are well

B–24

below the signal levels for the coronal observations. EUV observations are further hampered by the low reflectivity of optical coatings, and by the relatively high levels of scattering from optical surfaces at EUV wavelengths.

Figure B.6.1 provides a schematic diagram of the optical arrangement for the EUV Imager/Spectrograph which overcomes these difficulties. The telescope mirror is arranged so that the P/OF mask casts a shadow (geometrical shadow line in Figure B.6.1) that passes by the mirror at a distance of 2.3 cm. The telescope mirror is fully vignetted for observations within 1.1 solar radii of sun center and is filled for observations beyond 3.1 solar radii. Observations down to the limb and onto the solar disk can be accomplished with partial external occulting.

The telescope produces an image of the extended corona on the spectrograph entrance slit. The mirror is rotated to select the portion of the coronal image that passes through the slit and into the spectrograph. The telescope also forms an image of the external occulter inside the spectrograph. The spectrograph slit jaws intercept most of the light that is specularly reflected by the telescope toward that image. A linear internal occulter, located near the mirror face, blocks the diffracted light that would otherwise be specularly reflected through the spectrograph slit by the telescope. This internal occulter is translated across the face of the mirror as it is rotated so as to always intercept the specularly reflected light that would enter the slit. The telescope mirror must be highly polished in order to reduce the nonspecular reflection of the diffracted light to acceptable levels.

An illustration of the EUV Imager/Spectrograph is also provided in Figure B.6.1. A rectangular light baffle which is illuminated by direct sunlight on three sides and shadowed by the external occulter on the fourth, acts as an entrance aperture to the telescope/spectrograph enclosure. Direct sunlight passes through this aperture and is discarded by a reflector. An entrance slit baffle and the telescope mirror shield the entrance slit from light scattered by the reflector.

The telescope has a focal length of 3.5 meters. The Spectrometer has a 1.5–meter Rowland circle mount with an aspheric reflectance grating that provides stigmatic imagery. The spectral range from 1400 to less than 500 Å is accessible. Two–dimensional array detectors placed at selected spectral lines (e.g., HI Ly–α, OVI λ1032, and MgX λ610) provide simultaneous observations of spectral/spatial elements over 24 arc minute by 60 Å fields. The image scale is 1.02 mm/arc minute, and the reciprocal dispersion is 2.81 Å/mm. Detector pixels of 0.025 mm would provide spectral/spatial resolution elements of 0.07 Å and 1.47 arc seconds respectively. Time resolutions as short as 1 second are possible for an instantaneous field-of-view of 24 arc minutes by 10 arc seconds, and rasters of 24 $\times$ 24 arc minute sectors of the corona can be built–up in about 2 minutes.

B.6.3 Status of technology

The EUV Imager/Spectrograph is based on the design of the Ultraviolet Coronagraph–Spectrometer (Kohl, Reeves and Kirkham, 1978) that was flown successfully on sounding rockets. The present concept of the EUV Imager/Spectrograph scales the occulted

telescope of the rocket instrument by a factor of 20.

Although the instrument could take full advantage of several technological advances, existing technology combined with the P/OF opportunity would provide a factor of over 100 improvement in sensitivity for EUV spectroscopy of the extended corona. Technology areas relevant to the EUV Imager/Spectrograph include the following: two-dimensional array detectors for the EUV, high reflectance coatings for mirrors and gratings, aberration corrected reflectance gratings and superpolished mirrors.

Table B.6.1. Characteristics of the EUV Imager/Spectrograph

Aperture	50 cm
Image Scale	1.02 mm/arc min
Instantaneous Field-of-View	14 arc min × 1.5-10 arc sec
Field of Regard	0-10 solar radii from sun-center
Reciprocal Dispersion	2.81 Å/mm
Spectral Range	500-1400 Å
Temporal Resolution	1 sec (24 arc min × 10 arc sec in Ly-α)
Detector Type	1024 × 1024 microchannel array
Overall Dimensions	5.7 m × 0.64 m ×1.4 m
Mass	410 kg
Power	140 watts
Telemetry Rate	0.2 Mbps

EUV IMAGER/SPECTROGRAPH

ENTRANCE APERTURE

UNITS ARE CM

574

295.4

SPECTROMETER

TELESCOPE MIRROR

from $\rho = 1.5\ R_o$

from $\rho = 1.1\ R_o$

from SOLAR LIMB

EXTERNAL OCCULTER

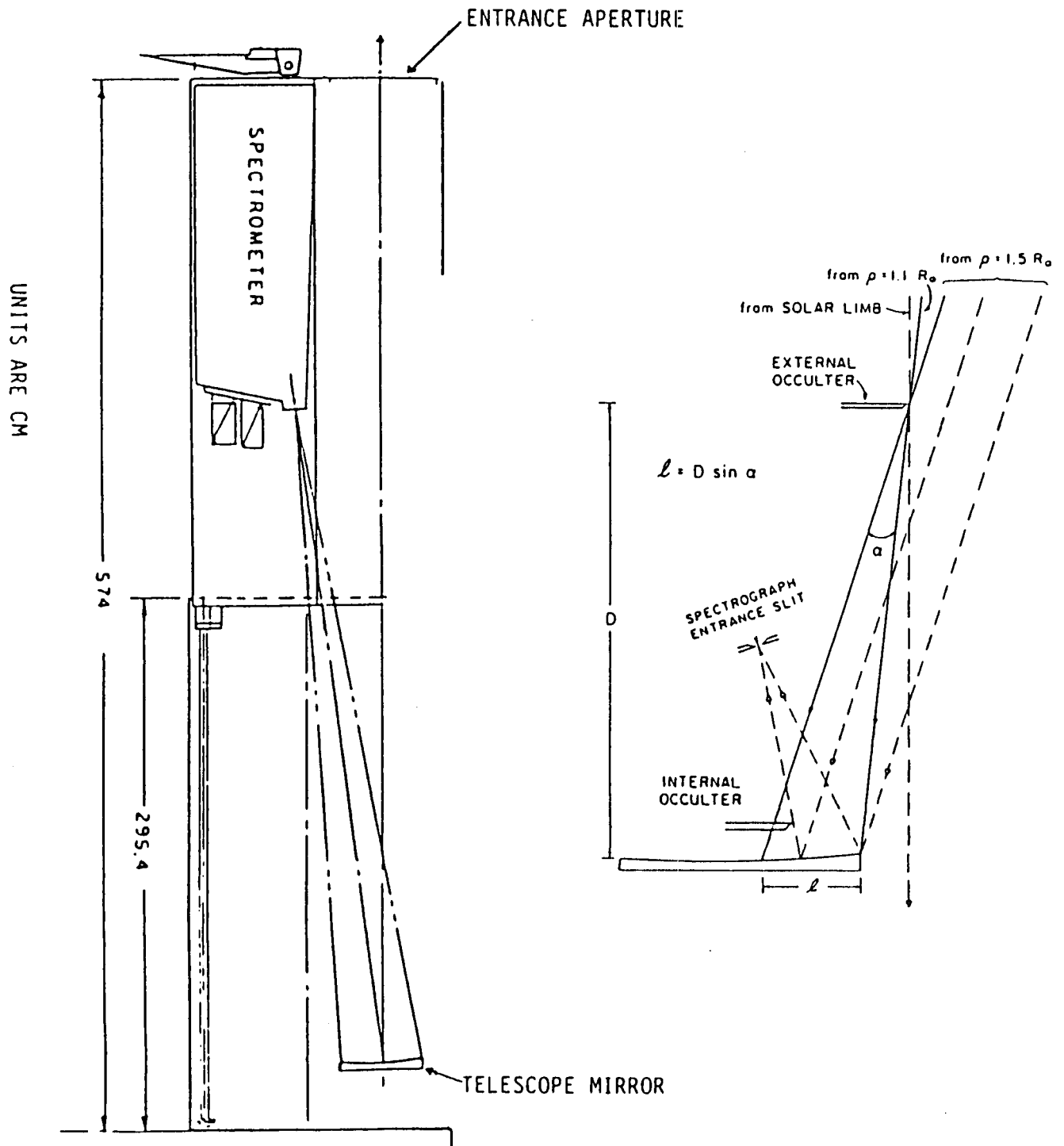$\ell = D \sin \alpha$

α

SPECTROGRAPH ENTRANCE SLIT

D

INTERNAL OCCULTER

γ

ℓ

Fig. 6.B.1. The telescope mirror of the EUV Imager/Spectrograph (left side of figure) is situated in the shadow of the remote P/OF mask. Direct light from the solar disk passes through the aperture and to the right of the mirror where it is reflected away by mirrors (not shown). The optical arrangement (not to scale), including the external occulter on the P/OF mask, is illustrated on the right.